JOURNAL OF PROPULSION AND POWER
Vol. 32, No. 3, May-June 2016

Coaxial Jet Flame Subject to Long-Wavelength Acoustic Oscillations

William A. Sirignano* and Jeremy Krieg†
University of California, Irvine, California 92697

DOI: 10.2514/1.B35953

A linear model is developed to relate the response of energy release rate per unit volume to velocity and pressure oscillations in a liquid-propellant rocket engine. Coaxial injection of fuel (outer flow) and oxygen (inner flow) is considered with chemical reaction in a thin flame and turbulent mixing as the controlling factor in an axisymmetric diffusion flame. The combustion process has a characteristic time for mixing, producing a time lag in the energy release rate relative to pressure. The model applies to an individual injector but can be used to couple the multipoint combustion processes and wave dynamics for a multi-injector chamber. In particular, the impacts of long-wavelength oscillations of pressure and velocity in the surrounding chamber gas on the mixing and burning rates are determined. The results are developed in a way that feedback to the chamber oscillations can be determined for either a computational analysis or a perturbation analysis of the chamber wave dynamics. Both the steady-state behavior and the unsteady linear perturbation for the coaxial jet are studied using an axisymmetric Green's function. Flame temperature, flame shape, and burning rates are found as a function of mixture ratio and injector size (mixing time). The combustion response factor for oscillatory behavior is also determined.

Nomenclature

A	=	pressure oscillation amplitude
a	=	speed of sound, m/s
c_p	=	specific heat at constant pressure, J/(kg · K)
c_v	=	specific heat at constant volume, J/(kg · K)
D	=	mass diffusivity, m^2/s
E	=	energy release rate per unit volume, $J/(m^3 \cdot s)$
f	=	frequency, s^{-1}
G	=	axisymmetric Green's function
g	=	gain for combustion response factor
h	=	specific enthalpy, J/kg
I_n	=	modified Bessel function of first kind and nth order
L_f	=	flame length, m
M	=	steady-state injector mass flow rate
$\dot{m}$	=	mass flow rate, kg/s
Pe	=	Peclet number
p	=	pressure, $N \cdot m^{-2}$
Q	=	energy value per mass of fuel, J/kg
$\dot{Q}$	=	energy release rate per mass of fuel, J/(kg · s)
R	=	chamber radius, m
$\boldsymbol{R}$	=	mixture specific gas constant, J/(kg · K)
R_f	=	flame radius, m
R_i	=	inner radius of coaxial jet, m
R_o	=	outer radius of coaxial jet, m
r	=	radial position, m
$r_{1/2}$	=	half-width of coaxial jet, m
St	=	Strouhal number
T	=	temperature, K
t	=	time, s
U	=	injector exit velocity, m/s
$\boldsymbol{u}$	=	vector velocity, m/s
$V_1(x)$	=	burning rate parameter, defined in Eq. (23), m^{-1}
$V_2(x)$	=	integral quantity, defined in Eq. (34)
$V_3(x)$	=	in-phase component of energy release rate factor, defined in Eq. (37)
$V_4(x)$	=	out-of-phase component of energy release rate factor, defined in Eq. (37)
x	=	streamwise position coordinate, m
α, β	=	Shvab–Zel'dovich variables
γ	=	ratio of specific heats
η	=	radial position, m
κ	=	variable defined after Eq. (1)
ν	=	kinematic viscosity, m^2/s (or fuel-to-oxygen mass stoichiometric ratio)
ρ	=	density, $kg \cdot m^{-3}$
τ	=	time lag, s
τ_M	=	characteristic mixing time, s
ϕ	=	phase for combustion response factor
ω	=	angular frequency, rad/s
ω_F	=	fuel reaction rate, rad/s

Subscripts

F	=	fuel
i	=	inflow condition
O	=	oxidizer
ss	=	steady state

Received 24 July 2015; revision received 11 October 2015; accepted for publication 16 October 2015; published online 8 January 2016.

*Professor, Department of Mechanical and Aerospace Engineering; sirignan@uci.edu. Fellow AIAA.

†Graduate Student Researcher, Department of Mechanical and Aerospace Engineering.

I. Introduction

HISTORICALLY, the research regarding the relation between combustion processes and acoustic oscillation may be traced back to the Rijke tube, named after its inventor in 1859, who discovered that acoustic oscillations can be excited in an open-ended vertical tube when a piece of fine wire mesh, heated by a gas flame placed underneath it, is stretched across the inside of the tube at certain positions in the lower half of the tube [1]. In 1979, Zinn et al. [2] modified the Rijke tube by replacing the wire mesh with a reserve of burning solid fuel and showed that acoustic oscillations can be excited in a Rijke tube driven by a combustion process. It was shown that the heat generated from the combustion process excites acoustic oscillations that improve the mixing process between the oxidizer and fuel. In 1989, Carvalho et al. [3] used the Rayleigh criterion to theoretically determine the locations where the heating element should be placed in a Rijke tube to achieve the maximum oscillation amplitude for each mode.

In the 1980s, McIntosh [4–6] studied acoustic wave and flame interactions in ducts and tubes for one-dimensional, anchored flames. Additional work with applications to a liquid-propellant rocket

engine (LPRE) analyzing acoustic instabilities for one-dimensional flames propagating in sprays and particle-laden flows is given by Clavin and Sun [7]. However, these one-dimensional flame analyses lack the necessary sophistication needed to model the diffusion flames encountered in turbulent LPRE combustion processes. General characteristics of diffusion flames as well as descriptions of the early analytical studies performed on steady-state diffusion flames are summarized by Williams [8].

Some of the early research on oscillating diffusion flames was performed in the 1960s by Strahle [9], who analyzed the frequency response for laminar jet diffusion-flame combustion by deriving an unsteady solution from linearization of a known steady-state boundary-layer solution. The physical structure and properties of diffusion flames were also studied a little later in time. For example, in 1973, Kent and Bilger [10] presented experimental results for the temperature distribution, flame composition, and flame shape of turbulent diffusion flames of a jet of hydrogen in a coaxial airstream.

In 1985, Sheshadri [11,12] analyzed diffusion flame stability by linearizing previous analytic results for steady-state diffusion flames [8] to obtain an eigenvalue problem. Neglecting viscosity and unsteady transport effects, Sheshadri predicted uniform unstable behavior for axisymmetric diffusion flames subject to axisymmetric disturbances [11]. Sheshadri also predicted that the growth of axisymmetric disturbances is approximately linear to the heat release from the flame [11]. The analysis was later expanded to include unsteady transport effects, and it was shown that the results reduce to the previous simplified case as the Peclet number is increased to infinity [12].

In the 1990s, Kim and Williams [13,14] studied strained diffusion flames in LPRE by modeling a turbulent combustion flame as an ensemble of laminar flamelets in a reaction sheet. They showed that the burning rate response is the most sensitive to acoustic pressure oscillations as the flame approaches extinction and stressed the importance of using finite chemical-reaction rates in the analysis to estimate more accurately the oscillation rate amplitudes. Sohn et al. [15] extended the analysis presented by Kim and Williams [13,14] to liquid droplet flames and showed that similar acoustic responses are obtained for both diffusion flames and droplet flames; however, the heat-release rate acoustic response is greater for strained diffusion flames than for droplet flames.

The essential features of transverse nonlinear oscillations in cylindrical LPRE combustion chambers have been captured in a model by Sirignano and Popov [16]. They analyzed stability and triggered instability by methods of computational fluid dynamics. The multiscale model included a system of equations describing the larger-scale, inviscid wave dynamics and a system of equations for each coaxial injector describing the turbulent jet diffusion flame. A two-dimensional, unsteady chamber-wave-dynamics model was developed by integrating the original three-dimensional equations over the axial direction. Nonlinear, first-tangential-mode wave oscillations in the circular combustion chamber were considered with the primary flow in the axial direction. Extensions of the model to include coupled injector flows, effects of motor acceleration, and rectangular chamber cross sections as well as experimental justification and stochastic analysis of several triggering mechanisms were developed by Popov et al. [17–20].

The Sirignano and Popov model of the coaxial jet flame [16] evolved as follows. In the earliest papers, axisymmetric configuration, Oseen approximation, one-step kinetics, and eddy diffusivity dependence only on axial jet velocity were taken [16,17]. Injector coupling, axisymmetric Reynolds-averaged Navier–Stokes (RANS), replacing the Oseen approximation, and eddy diffusivity dependence on both axial jet velocity and transverse wave velocity were added next [18]. The coaxial model was used in a study of transverse wave dynamics in a rectangular chamber [20]. Two-step kinetics now with use of flamelet PDFs and eddy diffusivity obtained from rapid distortion theory were used in that development. Favorable comparisons for the rectangular chamber were made with the results of a Purdue University experiment [21].

In a more recent work, Sirignano and Krieg [22] use the Sirignano and Popov [16] model as the basis for study of nonlinear, transverse-mode, LPRE combustion instability via a two-time-variable perturbation expansion in an amplitude parameter. Both triggered and spontaneous instability domains are studied. Two coupled first-order ordinary differential equations are developed and solved to predict amplitude and phase angle variations in the slow time for the major component of the waveform in an eigenfunction series expansion. Limit cycles and transient behaviors are resolved. Nonlinear triggering can occur in certain operational domains: above a critical initial amplitude, the amplitude grows; otherwise, it decays with time. Here, in this paper, the goal is to develop via closed-form analysis a model of the oscillatory coaxial jet that can be used to provide the energy release rate for the coupling of the combustion process with the perturbation model of the chamber wave dynamics. A linear treatment of combustion has been shown [22,23] to be sufficient for matching a nonlinear transverse wave oscillation in a circular LPRE chamber to third order in an expansion in the amplitude parameter. Therefore, both linear and nonlinear (triggered) combustion instabilities may be studied using the model developed here.

Although this work was originally motivated by the need for a simplified coaxial, oscillatory, diffusion-flame model for the aforementioned combustion-instability perturbation analysis [22], the model is capable of wider use.

II. Coaxial Flame Analysis

The wave dynamics equation [16,22] includes a term with the first time derivative of E, the rate of energy conversion per unit volume. This quantity E will oscillate when acoustic oscillations occur. The spatial scale of E is determined by injector and flame scales, whereas the scale (i.e., wavelength) of the acoustics is determined by the much larger chamber size. Thus, we may consider pressure to be time-varying but approximately uniform in space across the flame region for an individual injector. A flame model is required to relate E to velocity and pressure; that model was also advanced by Sirignano and Popov [16] and will be followed here.

The effect is sought of the source term E on driving the acoustic oscillation. In particular, the long wavelength impact of that forcing term must be determined. That E term represents the rate of conversion of chemical energy to thermal energy and will create entropy. Under oscillation, it will create kinematic entropy waves as well as directly modifying the longer-wavelength acoustic oscillations. Those shorter-length kinematic waves have been filtered in the wave-dynamics equation [16,22] under the assumption that turbulent mixing eliminates quickly those short waves with higher gradients. We follow that assumption here and neglect entropy waves.

We analyze now an individual coaxial, mixing, and reacting gaseous axisymmetric propellant stream for an individual injector. Both the steady-state behavior and the unsteady perturbation are examined. The flame length is assumed to be shorter than the chamber length so that complete combustion of the lean propellant is achieved. To apply this model to a flame in a multi-injector combustor, flames from neighboring injectors should not overlap with other. Thus, each injector can be analyzed in an isolated manner, only being coupled through local oscillation in chamber pressure and velocity.

The simplification of constant c_p value for the mixture will be made and $h = c_p T$. Then, the energy equation becomes

$$\rho\frac{\partial T}{\partial t} + \rho\boldsymbol{u}\cdot\nabla T - \left(\frac{k}{c_p}\right)\nabla^2 T - \frac{1}{c_p}\frac{\partial p}{\partial t} = \rho\frac{\dot{Q}}{c_p} = \rho\frac{Q}{c_p}\omega_F \tag{1}$$

Approximating an isentropic relationship between pressure and density and defining $\kappa = T/T_{\mathrm{ss},\infty} - (p/p_{\mathrm{ss}})^{(\gamma-1)/\gamma}$, we find

$$\frac{\partial \kappa}{\partial t} + \boldsymbol{u}\cdot\nabla\kappa - D\nabla^2\kappa = \frac{Q}{c_p T_{\mathrm{ss}}}\omega_F \tag{2}$$

where we take D to be both the thermal eddy diffusivity and the mass eddy diffusivity. For the gas ambient to the mixing, reacting stream,

$\kappa = 0$. Some error is accepted when it is assumed that the isentropic relation for density applies throughout the mixing region; it is a good approximation for the ambient gas.

Consider now the mass diffusion, advection, and chemical reaction for each species. The species continuity equation for each species may be written as follows:

$$\frac{\partial Y_i}{\partial t} + \boldsymbol{u} \cdot \nabla Y_i - D\nabla^2 Y_i = \omega_i \tag{3}$$

If an infinite-rate chemical reaction is considered with the same diffusivity for fuel and oxygen, one can construct a Shvab–Zel'dovich variable $\alpha = Y_F - \nu Y_O$, where ν is the fuel-to-oxygen mass stoichiometric ratio. Similarly, one can define $\beta = (Q/(c_p T_{\mathrm{ss},\infty}))Y_F + \kappa$. For the gas ambient to the mixing, reacting stream, $\alpha = 0$ and $\beta = 0$.

Consider now a coaxial injector with axisymmetric behavior where the dependent variables are functions of t, x, and η. Following practice, oxygen flows in the interior region surrounded by the annular fuel flow. Fuel-rich mixture ratios are preferred in rocket engine practice because the lower-molecular-weight products yield a little higher thrust; also, it desirable to keep oxygen away from the chamber walls. The dividing cylindrical barrier within the injector is assumed to be of zero thickness. See Fig. 1.

Gaseous oxygen flows from an injector at $x = 0$ for $0 \le \eta \le R_i$, whereas gaseous fuel flows through the injector at $x = 0$ for $R_i \le \eta \le R_o$. Following Sirignano and Popov [16] and Popov et al. [17], an Oseen approximation is made for the velocity field with uniform velocity $U(t)$ in the x direction. Velocities and densities of both streams are taken to be identical, although they differ in practice. Diffusion in the streamwise direction will be neglected. There is some similarity here between our coaxial configuration and the one chosen by Burke and Schumann in their classical work discussed by Williams [8]. Important differences are that now the coaxial streams have no wall boundary in the radial direction and the analysis is extended to the unsteady state. These simplifying assumptions allow analytical treatment, which is the goal here. They were used in previous computational fluid dynamics (CFD) analysis [16,17] and later relaxed with more exact treatments [18–20]. There was no qualitative difference in those CFD results for transverse combustion instability. Thus, we are comfortable that qualitative accuracy is not being sacrificed and trends can be identified.

The diffusivity is approximated as a spatially uniform, temporal function due to turbulence modulation. The estimate is based on the turbulent viscosity approximation for a self-similar turbulent jet [24]:

$$\nu_T = \frac{U_0(x) r_{1/2}(x)}{35} \tag{4}$$

where in Eq. (4) $U(t)$ is substituted for the centerline velocity $U_0(x)$, and R_o replaces the jet's half-width. Furthermore, the standard value of 0.7 is used for the turbulent Prandtl number, which yields

$$D = \frac{U(t) R_o}{24.5} \tag{5}$$

The implication here is that the turbulent Peclet number $Pe = UR_o/D = 24.5$.

The Oseen approximation, eddy-diffusivity approximation, and boundary- or mixing-layer approximation used here are well established in the literature. For example, the classical Burke–Schumann analysis follows this assumption [8]. Variations in the velocity and turbulent diffusivity and diffusion in the main flow direction will cause quantitative corrections but no qualitative corrections are expected. The approximation implies that the ambient combustion-chamber gas will recirculate and parallel the injected propellants at the same velocity. The governing equations become

$$\frac{\partial \alpha}{\partial t} + U(t)\frac{\partial \alpha}{\partial x} - D\left[\frac{\partial^2 \alpha}{\partial \eta^2} + \frac{1}{\eta}\frac{\partial \alpha}{\partial \eta}\right] = 0 \tag{6}$$

and

$$\frac{\partial \beta}{\partial t} + U(t)\frac{\partial \beta}{\partial x} - D\left[\frac{\partial^2 \beta}{\partial \eta^2} + \frac{1}{\eta}\frac{\partial \beta}{\partial \eta}\right] = 0 \tag{7}$$

The ambient boundary conditions are $\alpha(t, x, \infty) = \beta(t, x, \infty) = 0$. Boundary conditions are needed at $x = 0$. Consider that, for $0 \le \eta \le R_i$, $T(t, 0, \eta) = T_i(t)$, $Y_O(t, 0, r) = Y_{O,i}(t)$, $Y_F(t, 0, \eta) = 0$, $\kappa(t, 0, \eta) = T_i/T_{\mathrm{ss},\infty} - (p/p_{\mathrm{ss}})^{(\gamma-1)/\gamma}$, $\alpha(t, 0, \eta) = -\nu Y_{O,i}(t) \equiv f(t)$, $\beta(t, 0, \eta) = (p/p_{\mathrm{ss}})^{(\gamma-1)/\gamma} - T_i/T_{\mathrm{ss},\infty} \equiv g(t)$. For $R_i \le \eta \le R_o$, $T(t, 0, \eta) = T_i(t)$, $Y_O(t, 0, \eta) = 0$, $Y_F(t, 0, \eta) = Y_{F,i}(t)$, $\kappa = T_i/T_{\mathrm{ss},\infty} - (p/p_{\mathrm{ss}})^{(\gamma-1)/\gamma}$, $\alpha(t, 0, \eta) = Y_{F,o}$, and $\beta = (Q/(c_p T_{\mathrm{ss}}))Y_{F,i} + (p/p_{\mathrm{ss}})^{(\gamma-1)/\gamma} - T_i/T_{\mathrm{ss}}$. For $\eta \ge R_o$, $Y_O(t, 0, \eta) = Y_F(t, 0, \eta) = 0$, $\kappa(t, 0, R) = 0$, $\alpha(t, 0, \eta) = 0$, and $\beta(t, 0, \eta) = 0$, where $p(t, 0, \eta)$ and $T(t, 0, \eta)$ have the ambient values.

The scaling still has the pressure wavelength much larger than the domain under study here; the acoustic wavelength is O (100 cm) near the wall, whereas diffusion layers are of O (1 cm), and reactions zones are even smaller. Thus, the pressure may be considered uniform (over the domain of an individual injector but varying from one injector to another), although mass fractions and temperature will vary spatially and temporally due to the combined effects of heat and mass diffusion, convection or advection, and compression or expansion. The time for an acoustic wave to propagate through a single injector region is smaller than or comparable to the time for diffusion and reaction in that region. The wave speed order of magnitude is 10^2 to 10^3 m/s over a centimeter or so in the transverse dimension for a time between $O(10^{-5}$ s) and $O(10^{-4}$ s); the combustion times are about 10^{-4} s. Thus, the time variation of pressure is important for the combustion dynamics.

These equations impose a characteristic time for mixing. This characteristic mixing time τ_M does not appear explicitly in the calculations but implicitly will result in a time lag for the response of heat release to the pressure oscillation. An approximation for that mixing time is given by

$$\tau_M = (R_o - R_i)^2/D \tag{8}$$

In a perturbation analysis, the separation of steady-state term and linear perturbation term is necessary: $U(t) = \bar{U} + U'(t)$,

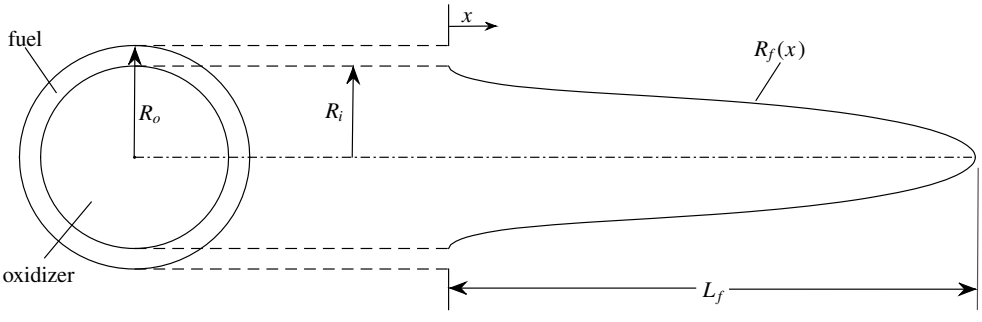

Fig. 1 Sketch of coaxial injector exit (left) and flame shape (right) for fuel-rich case.

$D(t) = \bar{D} + D'(t)$, $\alpha = \bar{\alpha}(\eta, x) + \alpha'(t, \eta, x)$, and $\beta(t, \eta, x) = \bar{\beta}(\eta, x) + \beta'(t, \eta, x)$. From the definition of the eddy diffusivity, it follows that

$$D' = (\bar{D}/\bar{U})U' \tag{9}$$

In this model, the effect of the transverse velocity on the diffusivity is neglected; only axial velocity is considered. The equations governing the steady state become

$$\bar{U}\frac{\partial\bar{\alpha}}{\partial x} - \bar{D}\left[\frac{\partial^2\bar{\alpha}}{\partial\eta^2} + \frac{1}{\eta}\frac{\partial\bar{\alpha}}{\partial\eta}\right] = 0 \tag{10}$$

and

$$\bar{U}\frac{\partial\bar{\beta}}{\partial x} - \bar{D}\left[\frac{\partial^2\bar{\beta}}{\partial\eta^2} + \frac{1}{\eta}\frac{\partial\bar{\beta}}{\partial\eta}\right] = 0 \tag{11}$$

With substitution of Eqs. (9–11), the equations governing the linear perturbations become

$$\frac{\partial\alpha'}{\partial t} + \bar{U}\frac{\partial\alpha'}{\partial x} - \bar{D}\left[\frac{\partial^2\alpha'}{\partial\eta^2} + \frac{1}{\eta}\frac{\partial\alpha'}{\partial\eta}\right] = -U'\frac{\partial\bar{\alpha}}{\partial x} + D'\left[\frac{\partial^2\bar{\alpha}}{\partial\eta^2} + \frac{1}{\eta}\frac{\partial\bar{\alpha}}{\partial\eta}\right] = 0 \tag{12}$$

and

$$\frac{\partial\beta'}{\partial t} + \bar{U}\frac{\partial\beta'}{\partial x} - \bar{D}\left[\frac{\partial^2\beta'}{\partial\eta^2} + \frac{1}{\eta}\frac{\partial\beta'}{\partial\eta}\right] = -U'\frac{\partial\bar{\beta}}{\partial x} + D'\left[\frac{\partial^2\bar{\beta}}{\partial\eta^2} + \frac{1}{\eta}\frac{\partial\bar{\beta}}{\partial\eta}\right] = 0 \tag{13}$$

Equations (6) and (7) have the same linear differential operator and are homogeneous. Physically, diffusion is occurring in individual axisymmetric planes that are advecting at velocity $U(t)$ in the x direction. Visualize a continual set of planes perpendicular to the x direction, which advect downstream from the injector face with a temporal diffusion within each of these planes. Thus, one may convert the two first-derivative terms into a Lagrangian time-derivative term. That is, define $\tilde{t} = t - \tau = \int \mathrm{d}x/U$, where τ is the time when mass in the particular plane was injected. Then, the equations become

$$\frac{\partial\alpha}{\partial\tilde{t}} - D\left[\frac{\partial^2\alpha}{\partial\eta^2} + \frac{1}{\eta}\frac{\partial\alpha}{\partial\eta}\right] = 0 \tag{14}$$

and

$$\frac{\partial\beta}{\partial\tilde{t}} - D\left[\frac{\partial^2\beta}{\partial\eta^2} + \frac{1}{\eta}\frac{\partial\beta}{\partial\eta}\right] = 0 \tag{15}$$

The boundary conditions at $x = 0$ can now be converted to initial conditions. That is, the boundary values at the instant when the element of mass was injected are the initial conditions for the diffusion plane to be solved for each of the plane (perpendicular to the x direction), which continually emerge from the injector face and advect downstream.

The Green's function $G(\eta, t; \xi, \tilde{t})$ for the axisymmetric diffusion equation [25,26] may be used to solve this problem:

$$G(\eta, t; \xi, \tilde{t}) = \frac{1}{4\pi D(t - \tilde{t})} e^{\frac{-(\eta^2+\xi^2)}{4D(t-\tilde{t})}} I_0\left(\frac{\eta\xi}{2D(t - \tilde{t})}\right) \tag{16}$$

where I_0 is the modified Bessel function of first kind and zero order. Conditions at the injector at a time $\tilde{t}$ affect conditions downstream at the x position via advection after a time $\tau = x/U$.

The solutions to Eqs. (14) and (15) may be written as

$$\alpha(t, x, \eta) = 2\pi\int_0^{\infty} G(\eta, x; \xi)\alpha(t - \tau, 0, \xi)\xi\,\mathrm{d}\xi = 2\pi\int_0^{R_o} G(\eta, x; \xi)\alpha(t - \tau, 0, \xi)\xi\,\mathrm{d}\xi \tag{17}$$

and

$$\beta(t, x, \eta) = 2\pi\int_0^{\infty} G(\eta, x; \xi)\beta(t - \tau, 0, \xi)\xi\,\mathrm{d}\xi = 2\pi\int_0^{R_o} G(\eta, x; \xi)\beta(t - \tau, 0, \xi)\xi\,\mathrm{d}\xi \tag{18}$$

where $t - \tau = x/U$, so that

$$G(\eta, x; \xi) = \frac{1}{4\pi Dx/U} e^{\frac{-(\eta^2+\xi^2)}{4Dx/U}} I_0\left(\frac{\eta\xi}{2Dx/U}\right) \tag{19}$$

The conditions for α at $x = 0$ remain constant with time. For $0 \le \eta \le R_i$, $Y_O(t-\tau, 0, \eta) = Y_{O,i}$, $Y_F(t-\tau, 0, \eta) = 0$, $\alpha(t-\tau, 0, \xi) = -\nu Y_{O,i}$; thus, $\bar{\alpha}_i = -\nu Y_{O,i}$ and $\alpha'(t - \tau, 0, \xi) = 0$. For $R_i \le \eta \le R_o$, $Y_O(t - \tau, 0, \xi) = 0$, $Y_F(t - \tau, 0, \xi) = Y_{F,o}$; thus, $\bar{\alpha}_o = Y_{F,o}$ and $\alpha'(t - \tau, 0, \xi) = 0$. For $\eta \ge R_o$, $Y_O(t-\tau, 0, \xi) = Y_F(t-\tau, 0, \xi) = 0$, $\alpha(t-\tau, 0, \xi) = 0$; and consequently, $\bar{\alpha}(t-\tau, 0, \xi) = \alpha'(t-\tau, 0, \xi) = 0$ in that outer region. It follows that $\alpha' = 0$ throughout the domain.

A. Steady-State Solution

After integration of Eqs. (17) and (18), the steady-state solution is given. At the thin-flame position $R_f(x)$, the value of $\alpha = 0$. Thus, a nonlinear integral equation for $R_f(x)$ follows:

$$\begin{aligned}\alpha(t, x, R_f) &= 2\pi\int_0^{R_o} G(R_f, x; \xi)\alpha(x/U, 0, \xi)\xi\,\mathrm{d}\xi \\ &= \frac{1}{2Dx/U}\int_0^{R_o} e^{\frac{-(R_f^2+\xi^2)}{4Dx/U}} I_0\left(\frac{R_f\xi}{2Dx/U}\right)\alpha(x/U, 0, \xi)\xi\,\mathrm{d}\xi \\ &= Y_{F,o}\frac{1}{2Dx/U}\int_{R_i}^{R_o} e^{\frac{-(R_f^2+\xi^2)}{4Dx/U}} I_0\left(\frac{R_f\xi}{2Dx/U}\right)\xi\,\mathrm{d}\xi \\ &\quad - \nu Y_{O,i}\frac{1}{2Dx/U}\int_0^{R_i} e^{\frac{-(R_f^2+\xi^2)}{4Dx/U}} I_0\left(\frac{R_f\xi}{2Dx/U}\right)\xi\,\mathrm{d}\xi = 0\end{aligned} \tag{20}$$

Because the perturbation quantity $\alpha' = 0$, the value of R_f will apply through first order. For fuel-rich mixture ratios, the flame length L_f can be determined by setting $R_f = 0$ in the preceding equation and solving for the corresponding value of x. That is, $R_f(L_f) = 0$. For fuel-lean cases, the largest x value where $\alpha = 0$ will identify the downstream edge of the flame and the flame length. Our discussion will emphasize the more practical fuel-rich cases, but some attention will be given to stoichiometric and fuel-lean mixtures.

The burning rate will depend on the diffusion rate of α at the flame position. To differentiate Eq. (17), we use

$$\begin{aligned}\frac{\partial}{\partial\eta}G(\eta, x; \xi) &= -\frac{\eta}{8\pi(Dx/U)^2} e^{\frac{-(\eta^2+\xi^2)}{4Dx/U}} I_0\left(\frac{\eta\xi}{2Dx/U}\right) \\ &\quad + \frac{\xi}{8\pi(Dx/U)^2} e^{\frac{-(\eta^2+\xi^2)}{4Dx/U}} \frac{\partial I_0(\eta\xi/2Dx/U)}{\partial(\eta\xi/2Dx/U)} \\ &= -\frac{\eta}{8\pi(Dx/U)^2} e^{\frac{-(\eta^2+\xi^2)}{4Dx/U}} I_0\left(\frac{\eta\xi}{2Dx/U}\right) \\ &\quad + \frac{\xi}{8\pi(Dx/U)^2} e^{\frac{-(\eta^2+\xi^2)}{4Dx/U}} I_1\left(\frac{\eta\xi}{2Dx/U}\right) \\ &= -\frac{\eta}{2Dx/U}G(\eta, x; \xi) + \frac{\xi}{8\pi(Dx/U)^2} e^{\frac{-(\eta^2+\xi^2)}{4Dx/U}} I_1\left(\frac{\eta\xi}{2Dx/U}\right)\end{aligned} \tag{21}$$

Thus,

$$\frac{\partial\alpha(t,x,\eta)}{\partial\eta} = 2\pi\int_0^{R_o}\frac{\partial G(\eta,x;\xi)}{\partial\eta}\alpha(t-\tau,0,\xi)\xi\,\mathrm{d}\xi$$
$$= -\frac{\pi\eta}{Dx/U}\int_0^{R_o} G(\eta,x;\xi)\alpha(t-\tau,0,\xi)\xi\,\mathrm{d}\xi$$
$$+\frac{1}{4(Dx/U)^2}\int_0^{R_o} e^{\frac{-(\eta^2+\xi^2)}{4Dx/U}} I_1\left(\frac{\eta\xi}{2Dx/U}\right)\alpha(t-\tau,0,\xi)\xi^2\,\mathrm{d}\xi$$
$$= -\frac{\eta}{2Dx/U}\alpha(t,x,\eta) + \frac{1}{4(Dx/U)^2}\int_0^{R_o} e^{\frac{-(\eta^2+\xi^2)}{4Dx/U}}$$
$$\times I_1\left(\frac{\eta\xi}{2Dx/U}\right)\alpha(t-\tau,0,\xi)\xi^2\,\mathrm{d}\xi \tag{22}$$

Consequently, at the flame position $\eta = R_f$, the first term in the previous equation becomes zero, and we have

$$V_1(x) \equiv \left.\frac{\partial\alpha}{\partial\eta}\right|_{R_f}(x) = \frac{1}{4(Dx/U)^2}\int_0^{R_o} e^{\frac{-(R_f^2(x)+\xi^2)}{4Dx/U}} I_1\left(\frac{R_f(x)\xi}{2Dx/U}\right)$$
$$\times\alpha(t-\tau,0,\xi)\xi^2\,\mathrm{d}\xi$$
$$= \frac{Y_{F,o}}{4(Dx/U)^2}\int_{R_i}^{R_o} e^{\frac{-(R_f^2(x)+\xi^2)}{4Dx/U}} I_1\left(\frac{R_f(x)\xi}{2Dx/U}\right)\xi^2\,\mathrm{d}\xi$$
$$-\frac{\nu Y_{O,i}}{4(Dx/U)^2}\int_0^{R_i} e^{\frac{-(R_f^2(x)+\xi^2)}{4Dx/U}} I_1\left(\frac{R_f(x)\xi}{2Dx/U}\right)\xi^2\,\mathrm{d}\xi \tag{23}$$

The diffusion-controlled steady-state burning rate per unit flame-length in the x direction $\mathrm{d}\bar{\dot{m}}/\mathrm{d}x$ is given by

$$\frac{\mathrm{d}\bar{\dot{m}}}{\mathrm{d}x} = 2\pi R_f\bar{\rho}_f\bar{D}\left.\frac{\partial\alpha}{\partial\eta}\right|_{R_f} = 2\pi R_f\frac{p_{\mathrm{ss}}}{\mathbf{R}\bar{T}_f}\bar{D}\left.\frac{\partial\alpha}{\partial\eta}\right|_{R_f}$$
$$= 2\pi\bar{D}\frac{p_{\mathrm{ss}}}{\mathbf{R}}\frac{R_f(x)V_1(x)}{\bar{T}_f(x)} \tag{24}$$

At $x = 0$, the change in α occurs across a diffusion layer of zero thickness. The singularity at $x = 0$ is a standard result under the boundary-layer (or mixing-layer) assumption. Thus, its appearance is ubiquitous in the literature. For example, note the famous Burke–Schumann problem [8]. The saving characteristic is that the singularity is integrable. By integrating over the flame length L_f, the finite total steady-state fuel mass burning rate associated with the injector is given as

$$\dot{M} \equiv \bar{\dot{m}}(L_f) = 2\pi\bar{D}\frac{p_{\mathrm{ss}}}{\mathbf{R}}\int_0^{L_f}\frac{R_f(x)V_1(x)}{\bar{T}_f(x)}\,\mathrm{d}x \tag{25}$$

The total chamber fuel mass burning rate with N identical injectors is $N\dot{M}$. The total mass flow rate for injection at stoichiometric portions would be $[(\nu+1)/\nu]N\dot{M}$. However, no assumption about overall mixture ratio has been made. Rich or lean flows can be included.

The solution for β is found in similar fashion. At the flame position, $Y_F = 0$, and we have

$$\beta(t,x,R_f) = \kappa(t,x,R_f) = \frac{Q}{c_pT_{\mathrm{ss},\infty}}Y_{F,o}\frac{1}{2Dx/U}\int_{R_i}^{R_o} e^{\frac{-(R_f^2+\xi^2)}{4Dx/U}}$$
$$\times I_0\left(\frac{R_f\xi}{2Dx/U}\right)\xi\,\mathrm{d}\xi$$
$$+\kappa(t-\tau,0)\frac{1}{2Dx/U}\int_0^{R_o} e^{\frac{-(R_f^2+\xi^2)}{4Dx/U}} I_0\left(\frac{R_f\xi}{2Dx/U}\right)\xi\,\mathrm{d}\xi \tag{26}$$

In the steady state,

$$\bar{\kappa}(x,R_f) = \frac{\bar{T}_f}{T_{\mathrm{ss},\infty}} - 1$$
$$= \frac{Q}{c_pT_{\mathrm{ss},\infty}}Y_{F,o}\frac{1}{2Dx/U}\int_{R_i}^{R_o} e^{\frac{-(R_f^2+\xi^2)}{4Dx/U}} I_0\left(\frac{R_f\xi}{2Dx/U}\right)\xi\,\mathrm{d}\xi$$
$$+\left[\frac{T_{i0}}{T_{\mathrm{ss},\infty}} - 1\right]\frac{1}{2Dx/U}\int_0^{R_o} e^{\frac{-(R_f^2+\xi^2)}{4Dx/U}} I_0\left(\frac{R_f\xi}{2Dx/U}\right)\xi\,\mathrm{d}\xi \tag{27}$$

yielding the steady-state solution for the flame temperature

$$\frac{\bar{T}_f(x)}{T_{\mathrm{ss},\infty}} = 1 + \frac{Q}{c_pT_{\mathrm{ss},\infty}}Y_{F,o}\frac{1}{2Dx/U}\int_{R_i}^{R_o} e^{\frac{-(R_f^2+\xi^2)}{4Dx/U}} I_0\left(\frac{R_f\xi}{2Dx/U}\right)\xi\,\mathrm{d}\xi$$
$$+\left[\frac{T_{i0}}{T_{\mathrm{ss},\infty}} - 1\right]\frac{1}{2Dx/U}\int_0^{R_o} e^{\frac{-(R_f^2+\xi^2)}{4Dx/U}} I_0\left(\frac{R_f\xi}{2Dx/U}\right)\xi\,\mathrm{d}\xi \tag{28}$$

B. Unsteady Perturbation Solution

The perturbation of mass fractions at the injector exit are zero, and the temperature fluctuation at that exit is isentropic; thus, the solution for the perturbation of β is given as

$$\beta'(t,x,\eta) = 2\pi\int_0^{R_o} G(\eta,x;\xi)\beta'(t-x/\bar{U},0,\xi)\xi\,\mathrm{d}\xi$$
$$= 2\pi\int_0^{R_o} G(\eta,x;\xi)\kappa'(t-x/\bar{U},0,\xi)\xi\,\mathrm{d}\xi$$
$$= 2\pi\int_0^{R_o} G(\eta,x;\xi)\frac{T'(t-x/\bar{U},0,\xi)}{T_{\mathrm{ss},\infty}}\xi\,\mathrm{d}\xi$$
$$-\frac{2\pi\gamma}{\gamma-1}\frac{p'(t-x/\bar{U})}{p_{ss}}\int_0^{R_o} G(\eta,x;\xi)\xi\,\mathrm{d}\xi$$
$$= \frac{2\pi\gamma}{\gamma-1}\left[\frac{T_{i0}}{T_{\mathrm{ss},\infty}} - 1\right]\frac{p'(t-x/\bar{U})}{p_{\mathrm{ss}}}\int_0^{R_o} G(\eta,x;\xi)\xi\,\mathrm{d}\xi \tag{29}$$

Given that the perturbations in α and flame radius R_f are zero-valued, the fluctuation in burning rate per unit length is

$$\frac{\mathrm{d}\dot{m}'}{\mathrm{d}x} = 2\pi\bar{D}\frac{p_{\mathrm{ss}}}{\mathbf{R}}\frac{R_f(x)V_1(x)}{\bar{T}_f(x)}\left[\frac{p'}{p_{\mathrm{ss}}} + \frac{D'}{\bar{D}} - \frac{T_f'}{\bar{T}_f}\right]$$
$$= 2\pi\bar{D}\frac{p_{\mathrm{ss}}}{\mathbf{R}}\frac{R_f(x)V_1(x)}{\bar{T}_f(x)}\left[\frac{p'}{p_{\mathrm{ss}}} + \frac{U'}{\bar{U}} - \frac{T_f'}{\bar{T}_f}\right] \tag{30}$$

The constant mass flux at the injector exit with isentropic fluctuation there yields that $U'/\bar{U} = -(1/\gamma)p'/p_{\mathrm{ss}}$. We consider here the effect of the variation in the jet velocity $U(t)$ due to the oscillation. The primary effect is through the density of the inflow, which is affected by pressure. The change in stagnation pressure due to transverse velocity fluctuation would have a second-order effect and is neglected. The influence of the transverse velocity on the turbulence in the jet and thereby on the diffusivity value is neglected here; in other works [18], it was considered without any qualitative differences.

From Eq. (29), the temperature fluctuation at the flame where mass fractions become zero may be determined as

$$\beta'(t,x,R_f) = \kappa'(t,x,R_f) = \frac{T_f'(t,x)}{T_{\mathrm{ss},\infty}} - \frac{\gamma-1}{\gamma}\frac{p'(t)}{p_{\mathrm{ss}}}$$
$$= \frac{2\pi\gamma}{\gamma-1}\left[\frac{T_{i0}}{T_{\mathrm{ss},\infty}} - 1\right]\frac{p'(t-x/\bar{U})}{p_{\mathrm{ss}}}\int_0^{R_o} G(R_f,x;\xi)\xi\,\mathrm{d}\xi \tag{31}$$

It follows that

$$\frac{T_f'(t,x)}{\bar{T}_f} = \frac{T_{ss,\infty}}{\bar{T}_f}\frac{\gamma-1}{\gamma}\frac{p'(t)}{p_{ss}} + \frac{T_{ss,\infty}}{\bar{T}_f}\frac{2\pi\gamma}{\gamma-1}\left[\frac{T_{i0}}{T_{ss,\infty}}-1\right] \times \frac{p'(t-x/\bar{U})}{p_{ss}}\int_0^{R_o} G(R_f,x;\xi)\xi\,\mathrm{d}\xi \tag{32}$$

Now,

$$\frac{\mathrm{d}\dot{m}'}{\mathrm{d}x} = \frac{\gamma-1}{\gamma}\frac{\mathrm{d}\bar{\dot{m}}}{\mathrm{d}x}\left(\left[1-\frac{T_{ss,\infty}}{\bar{T}_f(x)}\right]\frac{p'(t)}{p_{ss}} - \frac{T_{ss,\infty}}{\bar{T}_f(x)}\left[\frac{T_{i0}}{T_{ss,\infty}}-1\right] \times \frac{p'(t-x/\bar{U})}{p_{ss}}V_2(x)\right) \tag{33}$$

where

$$V_2(x) \equiv 2\pi\int_0^{R_o} G(R_f,x;\xi)\xi\,\mathrm{d}\xi \tag{34}$$

The integrated fuel-mass burning rate perturbation for the injector will depend on both the instantaneous pressure perturbation and the pressure perturbation at the time of injection for each discrete element of mass. Also, the integrated energy release rate perturbation is given by the product of Q and $\dot{m}'$. Namely,

$$\dot{E}' = Q\dot{m}'(t) = \frac{\gamma-1}{\gamma}\frac{p'(t)}{p_{ss}}\int_0^{L_f}\left(Q\frac{\mathrm{d}\bar{\dot{m}}}{\mathrm{d}x}\right)\left[1-\frac{T_{ss,\infty}}{\bar{T}_f(x)}\right]\mathrm{d}x - \frac{\gamma-1}{\gamma}\left[\frac{T_{i0}}{T_{ss,\infty}}-1\right] \times \int_0^{L_f}\frac{T_{ss,\infty}}{\bar{T}_f(x)}\frac{p'(t-x/\bar{U})}{p_{ss}}\left(Q\frac{\mathrm{d}\bar{\dot{m}}}{\mathrm{d}x}\right)V_2(x)\,\mathrm{d}x \tag{35}$$

The unsteady perturbation solution can be represented by defining a nondimensional combustion response factor, which is obtained from the ratio of the fuel-mass burning rate perturbation to the pressure perturbation. First, the integrated fuel-mass burning rate perturbation for the injector, given by Eq. (35), is normalized by the product $p_{ss}a_{ss}R^2$, where p_{ss}, a_{ss}, and R are, respectively, the steady-state (i.e., mean) pressure in the surrounding gas, the mean speed of sound in that gas, and the dimension (e.g., radius) of the chamber enclosing the surrounding gas. This quantity is then divided by the normalized pressure perturbation $p'(t)/p_{ss}$. The combustion response factor is analyzed for an imposed sinusoidal function of pressure $p'(t)/p_{ss} = Ae^{i\omega t}$, where A is any real nondimensional constant amplitude, and ω (in radians per second) is the perturbation frequency. The response factor consists of real and imaginary components. Now, considering only the real parts, $p'(t)/p_{ss} = A\cos(\omega t)$, and

$$\frac{\dot{E}'(t)}{p_{ss}a_{ss}R^2} = A[V_3\cos(\omega t) + V_4\sin(\omega t)] \tag{36}$$

where x and L_f are normalized by R and the definitions are given that

$$V_3(\omega x/\bar{U}) \equiv \frac{\gamma-1}{\gamma}\left(\int_0^{L_f}\left(\frac{Q}{p_{ss}a_{ss}R^2}\frac{\mathrm{d}\bar{\dot{m}}}{\mathrm{d}x}\right)\left[1-\frac{T_{ss,\infty}}{\bar{T}_f(x)}\right]\mathrm{d}x + \left[1-\frac{T_{i0}}{T_{ss,\infty}}\right]\int_0^{L_f}\frac{T_{ss,\infty}}{\bar{T}_f(x)}\cos(\omega x/\bar{U})\left(\frac{Q}{p_{ss}a_{ss}R^2}\frac{\mathrm{d}\bar{\dot{m}}}{\mathrm{d}x}\right)V_2(x)\,\mathrm{d}x\right)$$

$$V_4(\omega x/\bar{U}) \equiv \frac{\gamma-1}{\gamma}\left[1-\frac{T_{i0}}{T_{ss,\infty}}\right] \times \int_0^{L_f}\frac{T_{ss,\infty}}{\bar{T}_f(x)}\sin(\omega x/\bar{U})\left(\frac{Q}{p_{ss}a_{ss}R^2}\frac{\mathrm{d}\bar{\dot{m}}}{\mathrm{d}x}\right)V_2(x)\,\mathrm{d}x \tag{37}$$

The combustion response factor is the complex value $V_3 - iV_4$, where AV_3 and AV_4 are the amplitudes of the nondimensional burning rate (or nondimensional energy release rate) in phase and out of phase, respectively, with the pressure.

The equations and the computer code have been established in dimensional terms because the intention is to use them coupled with the analysis of wave dynamics in combustion chambers of varying sizes. One can easily convert the results to a nondimensional form using R_o, $R_o^2/\bar{D}$, and $\bar{D}/R_o$ for the reference length, time, and velocity, respectively. The steady-state value of the eddy diffusivity $\bar{D}$ is used here. Then, the key nondimensional parameters are radii ratio R_o/R_i, temperature ratio $T_{ss,\infty}/T_{i0}$, Peclet number $Pe = UR_o/D$, and Strouhal number $St = \omega R_o/\bar{U}$. Here, the steady-state value $\bar{U}$ is used. Through the constraints of Eqs. (5) and (9), the value of the Peclet number is fixed at $Pe = 24.5$ for both steady and unsteady conditions. A nondimensional mass flux can be created by using $\rho_{ss,\infty}\bar{D}R_o = [p_{ss}/(\mathbf{R}T_{ss,\infty})]\bar{D}R_o$ as a normalizing factor. Then, the nondimensional steady mass flow from the coaxial injector becomes $\pi Pe(T_{ss,\infty}/T_{i0})$.

III. Results

Calculations have been made to analyze both the steady-state and unsteady perturbation solutions for the coaxial flame. Results are presented here considering methane and gaseous-oxygen propellants with a base value for fuel-to-oxygen mass stoichiometric coefficient of 1/4. The ratio of specific heats $\gamma = 1.3$ and steady-state pressure of 200 atm have been chosen. For all calculations, the quantity $Q/(c_pT_{i0}) = 64.5$ remains constant. Under our assumptions about the same velocity and density for both propellants, the fuel-to-oxidizer mass mixture ratio is given by $\dot{M}_F/\dot{M}_O = (R_o/R_i)^2 - 1$, as shown in Fig. 2. The stoichiometric value of mixture ratio yields a radii ratio of 1.118.

Different cases are considered to gain a representative picture of the possible outcomes. First, a base case is considered with an outer injector radius of 1.1 cm and inner injector radius of 0.898 cm. The fuel and oxidizer leave the injector with an axial velocity of 200 m/s. Three parameter surveys are also performed. In one survey, the ratio of the outer injector radius to the inner injector radius (radii ratio) is kept fixed so that the mixture ratio is the same as in the base case. The magnitudes of the injector radii are varied, keeping the mass flux fixed (by fixing the factor $\bar{U}R_o^2$ or equivalently fixing $\bar{D}R_o$) with the same value as in the base case. The results show that, for a given radii ratio (or mixture ratio), the nondimensional results for various quantities fall on the same curve. See, for example, Fig. 3 for the nondimensional radial flame position, which is independent of injector size for a fixed radii ratio.

For another survey, the outer injector radius is kept at 1.1 cm with an axial velocity of 200 m/s. The mixture ratio is varied by changing the inner radius of the injector. From these calculations, one can infer the behavior of various nondimensional properties as functions of the ratio of outer radius to inner radius, R_o/R_i, or as functions of mixture

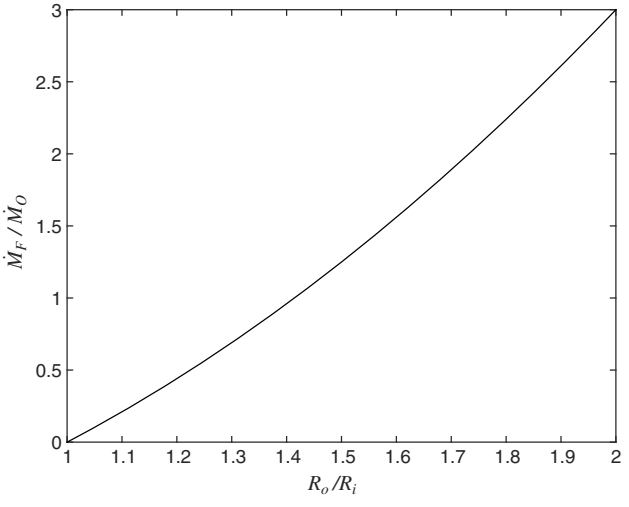

Fig. 2 Mixture ratio vs radii ratio.

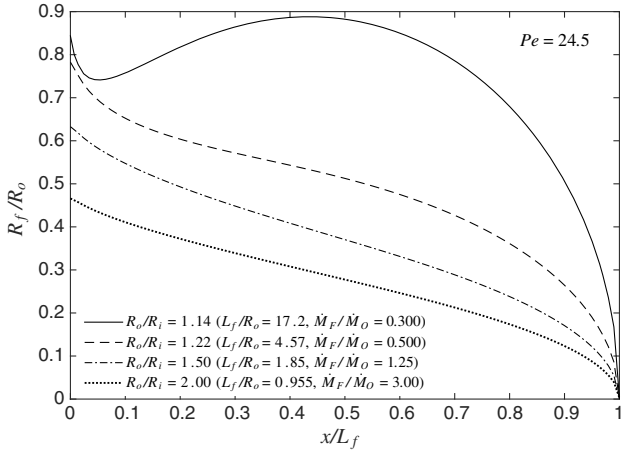

Fig. 3 Thin-flame position for fuel-rich mixtures.

ratio. For the final survey, the ratio of the steady-state ambient temperature to the initial injection temperature is varied, keeping the same injector radii and axial velocity as in the base case. In practice, a change of the inflowing mixture ratio will cause a change in the equilibrium temperature of the products, thereby coupling the parameters of the last two surveys; nevertheless, we treat them as distinct parameters here. The results presented in the following figures are for a single coaxial injector. The analysis has later been expanded to integrate several injectors with the chamber dynamics in a liquid-propellant rocket engine [22].

For the steady-state solution, Green's function is integrated numerically to evaluate the Shvab–Zel'dovich variable $\alpha(t, x, \eta)$. The thin-flame position $R_f(x)$ is obtained by setting $\alpha = 0$, and the flame length is obtained by finding the x position where $R_f = 0$. Figure 3 shows the thin-flame position for the overall study. At $x = 0$, the flame position has a value equal to the inner radius of the injector. For the base case, the corresponding flame length is about 5 cm. The calculations for the flame position and length do not depend on the temperature ratio $T_{ss,\infty}/T_{i0}$; thus, the results for the third survey are identical to the base case.

As shown in Fig. 3, variation of the mixture ratio has a significant effect on the thin flame distribution. For less fuel-rich mixtures, where the ratio of the outer to inner injector radius is small, the flame radial position reaches a local maximum downstream near the middle of the flame length instead of decreasing monotonically. For more fuel-rich mixtures, the flame radial position decreases with a nearly constant slope for the majority of the flame. All fuel-rich cases exhibit a sharp drop at the end of the flame, where the flame distribution has a vertical tangent. This is the more pronounced for less rich mixtures. The flame shapes in Fig. 3 are bell-shaped for fuel-rich mixtures; there is sufficient fuel to consume all of the oxygen, and no oxygen flows downstream of the flame. However, for a fuel-lean case, the shape is a truncated bell, with excess oxygen flowing through the opening in the flame near the axis (i.e., the flame radius does not decrease to zero anywhere, unlike the sketch shown in Fig. 1).

As the mixture becomes more rich, the amount of oxygen to be consumed in the flame decreases, and accordingly, the flame length decreases. As the stoichiometric value of 1.118 for the mixture ratio is approached, the flame length becomes very long because, after most of the fuel and oxygen are consumed, the radial gradients of both reactants become very small and the diffusion-controlled burning is slowed. The maximum flame radius increases as the mixture ratio approaches stoichiometric value. This behavior occurs because the fuel diffuses in both inward and outward radial directions. When the burning is slow, the center of the fuel mass fraction profile moves radially outward, bringing the flame outward as well. At the stoichoimetric mixture ratio value, the fuel diffuses so slowly that a finite flame length cannot be calculated.

Figure 4 shows the integrated burned fuel-mass flux between $x = 0$ and a given x position. As the radii ratio R_o/R_i is decreased at constant U and R_o, the inflowing mass flux of oxygen increases, whereas the inflowing mass flux of fuel decreases. For the fuel-lean cases portrayed on the left of Fig. 4, the fuel-mass burning rate has an asymptote that is approached faster in terms of downstream length as the amount of fuel is decreased. As the mixture ratio becomes more lean, there is less total fuel to be burned. Because the fuel burning-rate remains nonzero for increasing x, a finite flame length cannot be calculated for the fuel-lean cases. However, an effective flame length may be estimated from the burning-rate curve. For example, one could define the flame length as the x position where the fuel-mass burning rate reaches 99% of its asymptotic value. For the fuel-rich cases portrayed on the right of Fig. 4, all of the oxygen will burn but some fuel will be left unburned. The burning-rate curves therefore end at the x position corresponding to the flame length. For the fuel-rich mixtures, the burning-rate reaches zero slope at the end of the flame with a moderate length, whereas for the fuel-lean mixtures, the zero-slope is approached asymptotically but not reached for the length of our computational domain. The total amount of fuel that can be burned is proportional in the fuel-rich case to the total oxygen fuel. Therefore, with constant U and R_o, the total amount of fuel to be burned decreases with increasing mixture ratio although the total fuel mass inflow increases.

As the mixture ratio changes in either direction away from the 1.118 stoichiometric value, the radial gradient of one of the reactants becomes larger and drives the diffusion-controlled burning faster as indicated in Fig. 4. Thus, it takes a longer distance to complete combustion as the stoichiometric case is approached because gradients of both reactants get reduced as the reacting gas flows downstream. As noted previously, the fuel flow from the outer annulus diffuses radially in two directions: inward toward the flame and outward toward infinity; this aggravates the situation for the fuel-

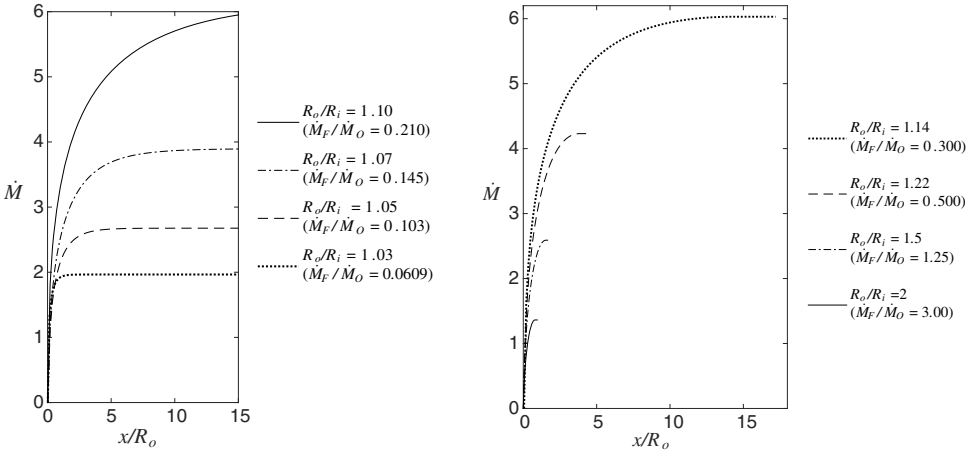

Fig. 4 Integrated steady-state fuel mass burning rate for a single injector for various mixture ratios as a function of downstream distance. Fuel-lean mixtures (left) and fuel-rich mixtures (right).

lean case because all of the fuel is needed to complete combustion, and the outward diffusion inhibits fast burning.

For a fixed mixture ratio, the dimensional flame length increases linearly with the injector outer radius when the mass flux factor $\bar{U}R_o^2$ is kept constant. The variation in the nondimensional flame length is given in Fig. 5 for fuel-rich mixtures. The variation in mixture ratio has a significant impact on the flame length. For fuel-rich mixtures approaching the stoichiometric value, the flame length increases exponentially due to the slowing of the diffusion-controlled burning. As the radii ratio increases, the flame length gradually decreases due to a decrease in the amount of available oxygen. For fuel-rich mixtures, the flame length is determined by the x position where the flame radial position $R_f(x)$ equals zero. For fuel-lean mixtures, when R_o/R_i moves below the stoichiometric value, the calculated flame position $R_f(x)$ does not reach zero, and excess oxygen can flow past the flame near the jet axis. An effective flame length for fuel-lean mixtures may be estimated from the fuel burning-rate curves, as described previously.

Results for $V_1(x)$, defined by Eq. (23), are given in Fig. 6, where we plot the nondimensional quantity R_oV_1, which is proportional to the rate at which mass diffuses into the flame per unit length of flame. Because the model assumes infinitely fast kinetics with diffusion control, $V_1(x)$ is proportional to the burning rate per unit length of flame. Figure 6 indicates that as stoichiometric conditions are approached, most of the burning is upstream with a low burning rate for the downstream portion of the flame. Consequently, as shown in the legend, a large flame length results. For all cases, V_1 has a singularity at $x = 0$ (due to the boundary-layer assumption) and approaches zero at the end of the flame. The value of V_1 at any given x position becomes larger as the outer injector radius is decreased and as the radii ratio is increased.

The nondimensional flame temperature distributions are given in Figs. 7 and 8. For all cases, there is an initial rise in temperature near $x = 0$, followed by a decrease in temperature, which approaches a constant value at the end of the flame. The magnitudes of the inner and outer injector radii do not affect the flame temperature as long as the mixture ratio is fixed. Thus, the variation of flame temperature with a nondimensional flame position is the same for a given mixture ratio regardless of the size of the injector. Essentially, the flame temperature as a function of x/L_f is unchanged, and L_f scales with R_o. Of course, the mixture ratio has a significant effect on the flame temperature. For less rich mixtures, the flame temperature varies more over the flame length and decreases with downstream position by a larger amount compared to the more fuel-rich cases. For more fuel-rich mixtures, the flame temperature varies less over the flame length. The more rich mixtures have larger concentration gradients, causing larger burning rates and completion of combustion in a shorter length. The amount of energy converted through the fuel-rich

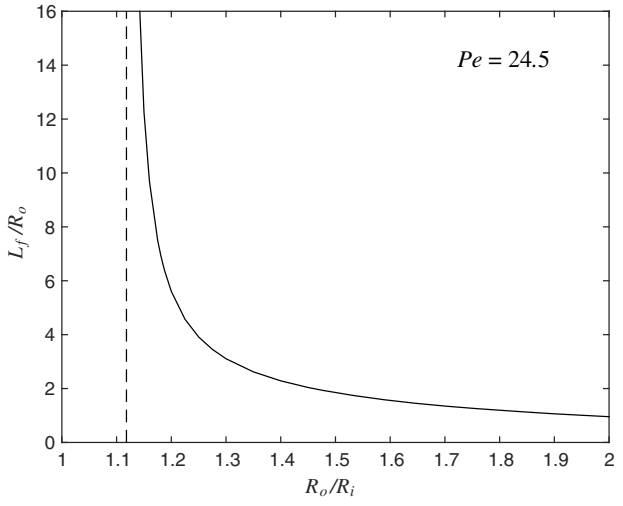

Fig. 5 Nondimensional flame-length variation for fuel-rich mixtures.

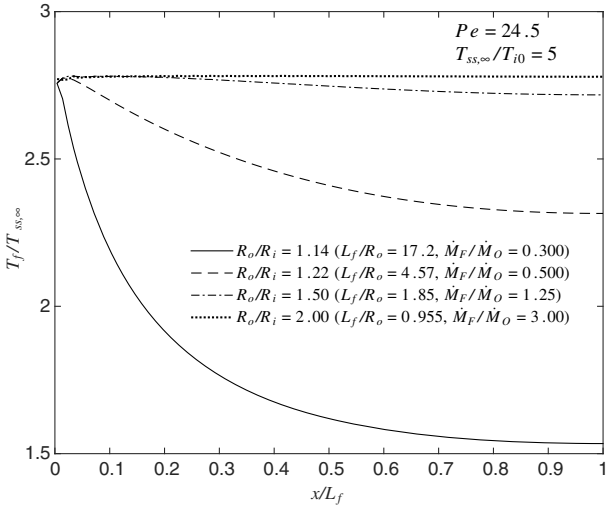

Fig. 7 Nondimensional flame-temperature distribution for various injectors and fuel-rich mixture ratios.

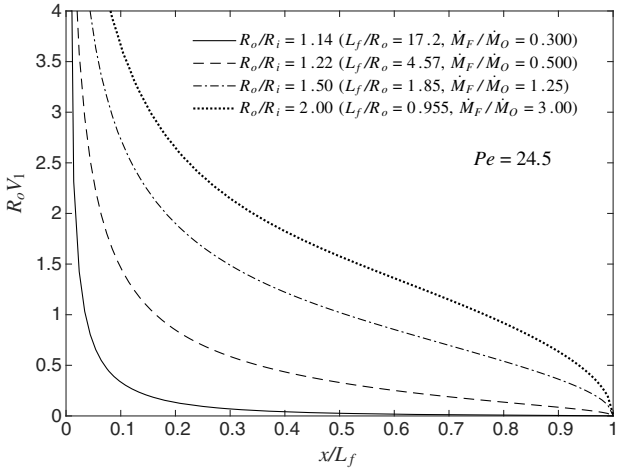

Fig. 6 Nondimensional burning-rate parameter R_oV_1 vs nondimensional downstream position x/L_f for fuel-rich mixtures.

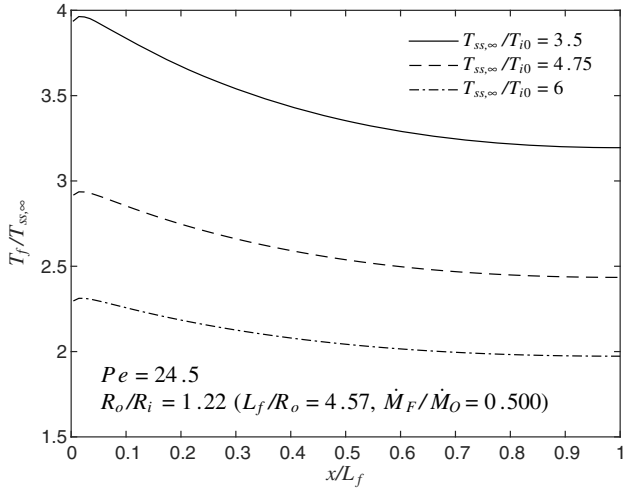

Fig. 8 Nondimensional flame-temperature distribution for various inflow and ambient temperatures.

domain is proportional to the total amount of oxygen reacted, which changes little with mixture ratio. Thus, for less-rich flames, the energy release is over a larger flame length, resulting in lower flame temperature. For a fixed mixture ratio, the nondimensional flame temperature in Fig. 8 increases with increasing temperature ratio $T_{ss,\infty}/T_{i0}$; physically, an increase in the inflow temperature simply results in an increase in the flame temperature.

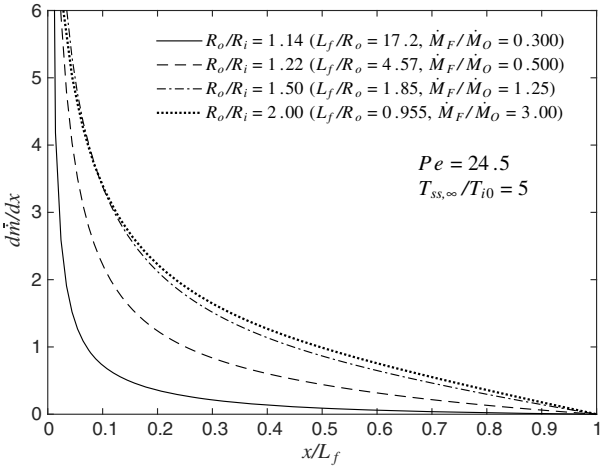

Fig. 9 Nondimensional steady-state fuel mass burning rate per unit flame-length for various injectors and fuel-rich mixture ratios.

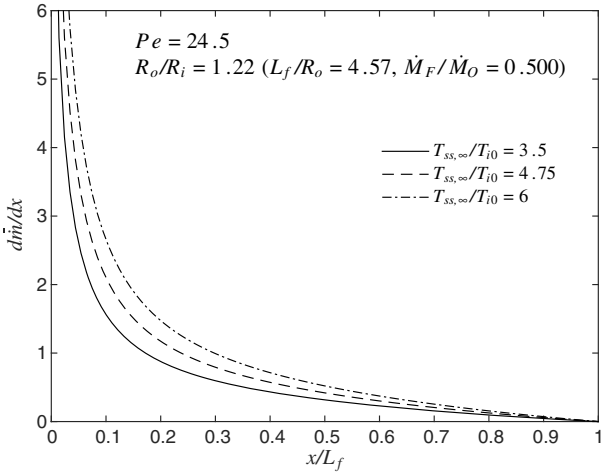

Fig. 10 Nondimensional steady-state fuel mass burning rate per unit flame-length for various inflow and ambient temperatures.

The diffusion-controlled steady-state fuel mass burning rate per unit flame-length in the x direction is shown in nondimensional form in Figs. 9 and 10 for the overall study. Similar to the curves for $V_1(x)$, there is a singularity at the beginning of the flame at $x = 0$. However, that singularity is integrable, giving a finite value for the overall burning rate. The burning rate decreases along the length of the flame and equals zero at the end of the flame, as expected. The effects of injector size and mixture ratio are similar to those exhibited by the curves for $V_1(x)$. As shown by Fig. 10, an increase in the temperature ratio $T_{ss,\infty}/T_{i0}$ increases the nondimensional mass burning rate without changing flame length. In reality, the dimensional burning rate would not change with fixed injector size as ambient temperature changes; the ambient density has been used in normalizing mass flux and causes the variation.

Figure 11 shows that the total mass burning rate in the flame decreases with the radii ratio and therefore with the mixture ratio. As noted earlier, as mixture ratio increases through the fuel-rich range, more fuel flows but less burns because there is less oxygen available. For a fixed mixture ratio, the nondimensional burning rate increases with temperature ratio, a consequence of the change in the density used for normalization.

The results presented so far have all dealt with the steady-state solution. Calculations are also performed to study the oscillating burning rate using the unsteady perturbation solution. For each of the different cases, the distribution $V_2(x)$, defined by Eq. (34), is given in Fig. 12. The distribution $V_2(x)$ is important because it has a significant effect on the combustion response factor, which is used to analyze the unsteady solution. The distribution has zero-valued slopes at $x = 0$, where $V_2 = 1$, and at the end of the flame. The flame length L_f and flame shape $R_f(x)$ scale with R_o and are not affected by the temperature ratio. Thus, $V_1(x)$ and $V_2(x)$ are also independent of the temperature ratio. They depend strongly on mixture ratio, which is varied through R_o/R_i. For the $V_2(x)$ distributions in Fig. 12, the effect of the change in mixture ratio is very similar to that observed for the flame temperature distribution.

The nondimensional combustion response factor provides some useful insight to the oscillatory behavior. Both the in-phase (V_3) and out-of-phase (V_4) components of the combustion response factor are given in Fig. 13 as functions of St, R_o/R_i, and $T_{ss,\infty}/T_{i0}$. The in-phase component decreases as the Strouhal number or frequency increases. The out-of-phase component reaches a local maximum at a certain frequency (approximately 16,000 rad/s in the base calculation) and then decreases as the frequency is further increased. This behavior indicates that, at lower frequencies, the energy release rate can more easily follow the changes in pressure during the oscillation. At larger frequencies, a significant lag can occur. The lag

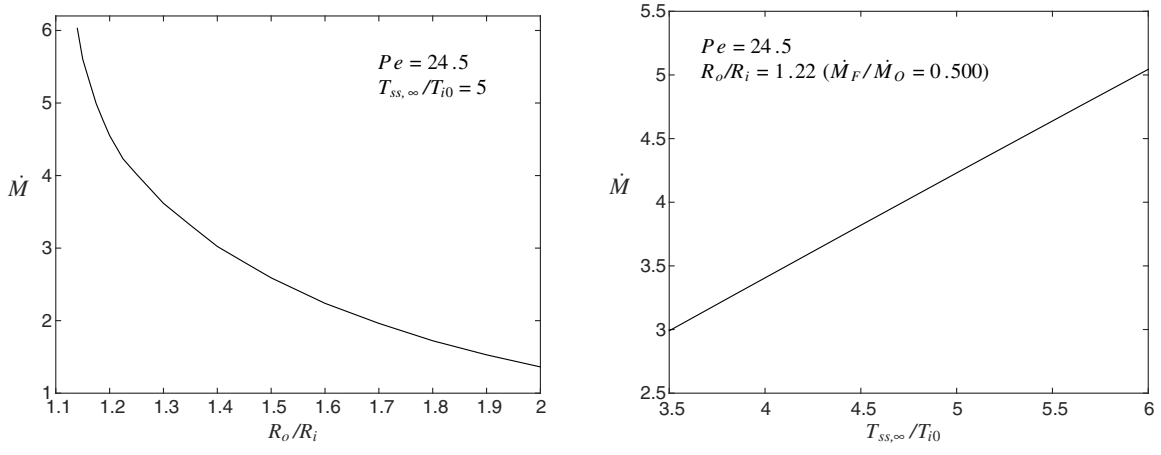

Fig. 11 Steady-state fuel mass burning rate for a single injector.

is expected because diffusion causes a history effect; as seen from Eqs. (33) and (35), the pressure oscillation at the injector exit at an earlier time affects the downstream burning rate at a later time. We expect that, at a lower frequency, there is less change in the pressure value during the time taken for the reactants to flow downstream from the injector exit, mix by diffusion, and react (i.e., from $t - x/\bar{U}$ to t).

The effects of injector size, mixture ratio, and temperature ratio are examined by evaluating the combustion response factor at a particular perturbation frequency. V_3 decreases as the radii ratio is increased. V_4 reaches a maximum at the radii ratio corresponding to the base case and then decreases as the ratio of the outer-to-inner injector radius is increased. V_3 decreases and V_4 increases in an approximately linear fashion as the temperature ratio $T_{ss,\infty}/T_{i0}$ increases. Again, note that, in a practical combustor, mixture ratio changes will cause changes in the gas ambient temperature where products of combustion exist. For example, as the mixture gets richer, a decrease in V_3 occurs due to increase in radii ratio, and an increase in V_3 occurs due to the associated temperature decrease. The actual effect of mixture ratio change would be determined from the combined effect.

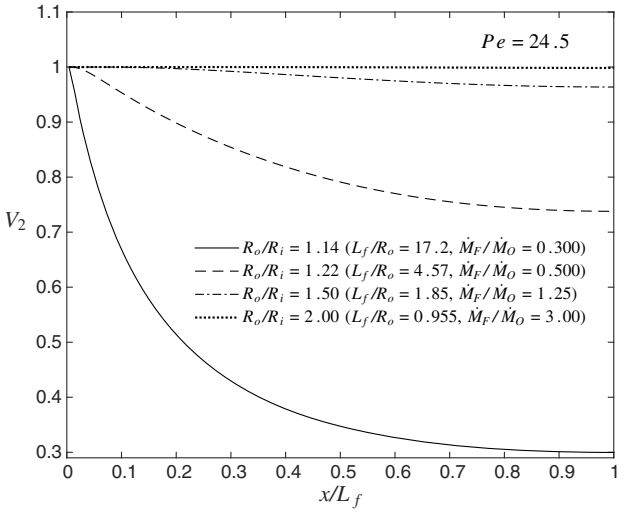

Fig. 12 Integral quantity $V_2(x)$ vs x/L_f.

The results are in qualitative agreement with the findings of Sirignano and Popov [16], who used the current model coupled with their wave dynamics for instabilities in a cylindrical rocket combustion chamber. For example, the situation becomes more stable as the mixture ratio deviates away from the stoichiometric value to a more rich case. The flame temperature and the energy release per unit mass of combustible mixture peak very near the stoichiometric point; thus, the behavior of the in-phase component V_3 in Fig. 13 is not surprising.

For many linear treatments of combustion instability, complex-variable notation is used, and the combustion response factor is converted to a form using gain g and phase ϕ, where $V_3 - iV_4 \equiv ge^{i\phi}$. In Fig. 14, g and ϕ are plotted versus various parameters. The results, of course, are consistent with those of Fig. 13. The gain-phase complex-variable notation is less useful in nonlinear analyses because squares and double products appear, which demand multiplication of only the real parts of the variables.

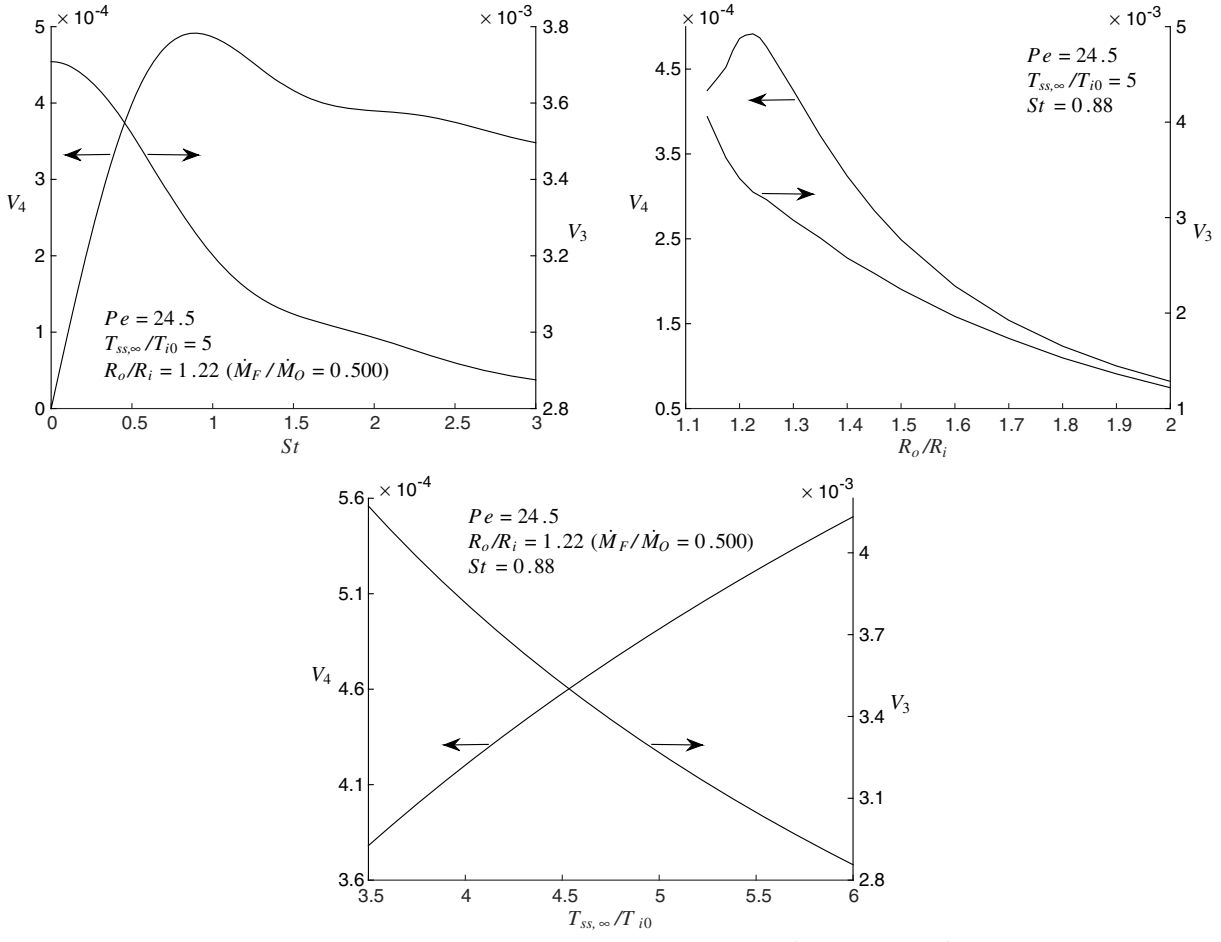

Fig. 13 V_3 and V_4 as functions of a) Strouhal number, b) R_o/R_i, and c) $T_{ss,\infty}/T_{i0}$.

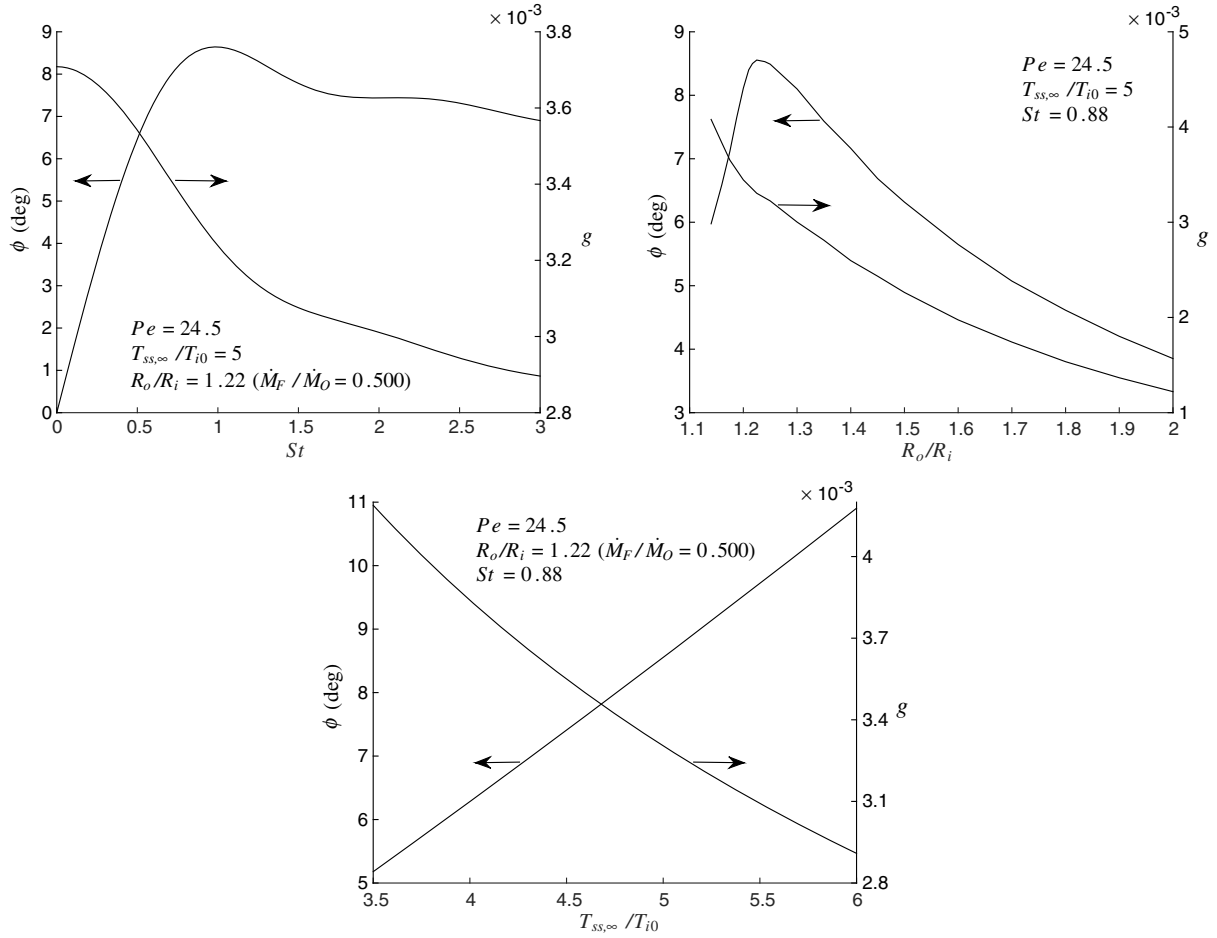

Fig. 14 Gain and phase as functions of a) Strouhal number, b) R_o/R_i, and c) $T_{ss,\infty}/T_{i0}$.

IV. Conclusions

A model has been developed to relate the fuel mass burning rate to long-wavelength pressure oscillations in a liquid-propellant rocket engine. An axisymmetric diffusion flame is used to model coaxial injection of fuel and oxygen in the combustion process. Both the steady-state behavior and unsteady perturbation are examined, using an Oseen approximation for the velocity field. The equations governing the linear perturbations are developed and solved using Green's function for the axisymmetric diffusion equation. The coaxial flame model applies to an individual injector in a liquid-propellant rocket engine combustion process; however, it has the potential for wider use in other applications where oscillating jet diffusion flames are present. In this configuration, the fuel-to-oxygen mass mixture ratio is a quadratic function of the ratio of the outer-to-inner radii of the coaxial injector.

Placement of the computational results in a nondimensional form has been useful and allows conclusions to cover a broader domain of the dimensional values. Five important nondimensional parameters have been identified. The turbulent Peclet number is held constant under empirical constraints found in the literature. The ratio of the outer to inner radii of the coaxial injector and the mixture ratio are directly related, leaving four independent parameters, with three of them not constrained by the model assumptions. Thus, radii ratio, the ratio of ambient temperature to inflow temperature, and the Strouhal number are surveyed.

The steady-state solution is used to compute the thin-flame radial position, flame length, temperature distribution, and steady-state fuel-mass burning rate. Results are examined for a range of different cases using typical values for the combustion parameters. A base case is considered as well as parameter surveys that vary the injector size, combustion mixture ratio, and the ratio of the ambient temperature to the inflow temperature. Several trends are predicted from the steady-state solution. For example, at a fixed mixture ratio, the flame length increases linearly with the injector size. The ratio of the flame length to the outer radius of the injector increases as the mixture becomes less fuel-rich. Consequently, the energy is released over a greater length, and the average flame temperature becomes lower as the mixture ratio deviates toward the stoichiometric value.

For the unsteady perturbation solution, a combustion response function is developed to relate the oscillating burning rate to an imposed pressure perturbation. Results for the in-phase and out-of-phase components of the response function are presented for a given cosinusoidal pressure perturbation. The in-phase component maximizes at zero frequency, indicating the most unstable frequency. It decreases with increasing frequency but still has a substantial value at the Strouhal number where the out-of-phase component has a maximum. The effects of injector size, mixture ratio, and temperature ratio are examined at this specific frequency where the out-of-phase component maximizes. The characteristic time for combustion (i.e., the time lag) will vary with these quantities. The interesting question is how that characteristic time compares with the period of oscillation. The Strouhal number is essentially a ratio of those two times. The indication is that the most unstable condition exists when the characteristic time is negligible compared to the oscillation period.

Sirignano and Krieg [22] recently used this linear coaxial flame model for a transverse combustion instability analysis; they obtained perturbation expansions up through third order in the amplitude magnitude expansion that are qualitatively consistent for certain trend predictions with previous computational fluid dynamics (CFD) analyses of transverse oscillations using a similar jet-flame model. Prior CFD calculations were first made using the Oseen approximation [16,17] and later with the full RANS representation [18–20]. This agreement indicates that the perturbation analysis is reliable as a simpler and less costly approach to predicting trends. For

example, Sirignano and Krieg more easily examined the consequences of varying the number of injectors in the chamber, an important issue that had not previously been examined.

Acknowledgments

This research was supported by the U.S. Air Force Office of Scientific Research under grants FA9550-12-1-0156 and FA9550-15-1-0033 with Mitat Birkan as the Program Manager.

References

[1] Rayleigh, J. W. S., *The Theory of Sound*, Vol. 32, 2nd ed., Macmillian, London, 1896, pp. 231–234.

[2] Zinn, B. T., Daniel, B. R., and Sheshadri, T. S., "Application of Pulsating Combustion in the Burning of Solid Fuels," *Proceedings of the Symposium on Pulse Combustion Technology for Heating Applications*, U.S. Department of Energy Rept. ANL/EES-TM-87, Lemont, IL, 1979, pp. 239–248.

[3] Carvalho, J. A., Ferreira, M. A., Bressan, C., and Ferreira, J. L. G., "Definition of Heater Location to Drive Maximum Amplitude Acoustic Oscillations in a Rijke Tube," *Combustion and Flame*, Vol. 76, No. 1, 1989, pp. 17–27. doi:10.1016/0010-2180(89)90073-4

[4] McIntosh, A. C., "The Effect of Upstream Acoustic Forcing and Feedback on the Stability and Resonance Behavior of Anchored Flames," *Combustion Science and Technology*, Vol. 49, Nos. 3–4, 1986, pp. 143–167. doi:10.1080/00102208608923908

[5] McIntosh, A. C., "Combustion-Acoustic Interaction of a Flat Flame Burner System Enclosed Within an Open Tube," *Combustion Science and Technology*, Vol. 54, Nos. 1–6, 1987, pp. 217–236. doi:10.1080/00102208708947054

[6] McIntosh, A. C., "On Flame Resonance in Tubes," *Combustion Science and Technology*, Vol. 69, Nos. 4–6, 1990, pp. 147–152. doi:10.1080/00102209008951607

[7] Clavin, P., and Sun, J., "Theory of Acoustic Instabilities of Planar Flames Propagating in Sprays or Particle-Laden Gases," *Combustion Science and Technology*, Vol. 78, Nos. 4–6, 1991, pp. 265–288. doi:10.1080/00102209108951752

[8] Williams, F. A., *Combustion Theory*, 2nd ed., Benjamin/Cummings Publ., Menlo Park, CA, 1985, pp. 38–51.

[9] Strahle, W. C., "Unsteady Laminar Jet Flame at Large Frequencies of Oscillation," *AIAA Journal*, Vol. 3, No. 5, 1965, pp. 957–960. doi:10.2514/3.3024

[10] Kent, J., and Bilger, R., "Turbulent Diffusion Flames," *Proceedings of the 14th Symposium (International) on Combustion*, Combustion Inst., Pittsburgh, PA, 1973, pp. 615–625.

[11] Sheshadri, T. S., "Stability Analysis of a Class of Diffusion Flames," *AIAA Journal*, Vol. 23, No. 1, 1985, pp. 88–94. doi:10.2514/3.8875

[12] Sheshadri, T. S., "Unsteady Transport Effects on Diffusion Flame Stability," *AIAA Journal*, Vol. 23, No. 12, 1985, pp. 1991–1993. doi:10.2514/3.9210

[13] Kim, J. S., and Williams, F. A., "Contribution of Strained Diffusion Flames to Acoustic Pressure Response," *Combustion and Flame*, Vol. 98, No. 3, 1994, pp. 279–299. doi:10.1016/0010-2180(94)90242-9

[14] Kim, J. S., and Williams, F. A., "Acoustic-Instability Boundaries in Liquid-Propellant Rockets: Theoretical Explanation of Empirical Correlation," *Journal of Propulsion and Power*, Vol. 12, No. 3, 1996, pp. 621–624. doi:10.2514/3.24081

[15] Sohn, C. H., Chung, S. H., Kim, J. S., and Williams, F. A., "Acoustic Response of Droplet Flames to Pressure Oscillations," *AIAA Journal*, Vol. 34, No. 9, 1996, pp. 1847–1854. doi:10.2514/3.13317

[16] Sirignano, W. A., and Popov, P. P., "Two-Dimensional Model for Liquid-Rocket Transverse Combustion Instability," *AIAA Journal*, Vol. 51, No. 12, 2013, pp. 2919–2934. doi:10.2514/1.J052512

[17] Popov, P. P., Sideris, A., and Sirignano, W. A., "Stochastic Modelling of Transverse Wave Instability in a Liquid-Propellant Rocket Engine," *Journal of Fluid Mechanics*, Vol. 745, 2014, pp. 62–91. doi:10.1017/jfm.2014.96

[18] Popov, P. P., Sirignano, W. A., and Sideris, A., "Propellant Injector Influence on Liquid-Propellant Rocket Engine Instability," *Journal of Propulsion and Power*, Vol. 31, No. 1, 2015, pp. 320–331. doi:10.2514/1.B35400

[19] Popov, P. P., Sideris, A., and Sirignano, W. A., "Triggering and Re-Stabilization of Combustion Instability with Rocket Motor Acceleration," *AIAA Journal* (to be published).

[20] Popov, P. P., and Sirignano, W. A., "Transverse Combustion Instability in a Rectangular Rocket Motor," *Journal of Propulsion and Power* (to be published).

[21] Shipley, K., Morgan, C., Anderson, W., Harvazinski, M., and Sankaran, V., "Computational and Experimental Investigation of Transverse Combustion Instabilities," *49th AIAA/ASME/SAE/ASEE Joint Propulsion Conference*, AIAA Paper 2013-3992, 2013.

[22] Sirignano, W. A., and Krieg, J., "Two-Time-Scale Perturbation Theory for Liquid-Rocket Combustion Instability," *Journal of Propulsion and Power* (to be published).

[23] Sirignano, W. A., "Driving Mechanisms for Combustion Instability," *Combustion Science and Technology*, Vol. 187, Nos. 1–2, 2015, pp. 162–205.

[24] Pope, S. B., *Turbulent Flows*, Cambridge Univ. Press, Cambridge, England, U.K., 2000, pp. 118–122.

[25] Duffy, D. G., *Green's Functions with Applications*, 2nd ed., CRC Press, Boca Raton, FL, 2015, pp. 283–290.

[26] Kythe, P. K., *Green's Functions and Linear Differential Equations: Theory, Applications, and Computation*, CRC Press, Boca Raton, FL, 2011, pp. 157–158.

J. C. Oefelein
Associate Editor